Building and Environment 215 (2022) 108969

Contents lists available at ScienceDirect

Building and Environment

journal homepage: www.elsevier.com/locate/buildenv

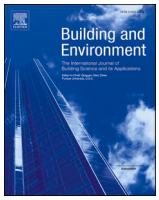

Parametric study on vertical void configurations for improving ventilation performance in the mid-rise apartment building

Nikhil Kumar [a], Ronita Bardhan [a,b], Tetsu Kubota [c,*], Yoshihide Tominaga [d], Mohammadreza Shirzadi [c,d]

[a] Centre for Urban Science and Engineering, Indian Institute of Technology, Bombay, 400076, Mumbai, India
[b] Department of Architecture, University of Cambridge, Cambridge, CB2 1PX, United Kingdom
[c] Graduate School of Advanced Science and Engineering, Hiroshima University, Higashi-Hiroshima, Japan
[d] Wind and Fluid Engineering Research Center, Niigata Institute of Technology, Kashiwazaki, Japan

ARTICLE INFO

Keywords:
Vertical void
Pilotis
Wind fin
Natural ventilation
CFD
Passive design

ABSTRACT

Double-loaded affordable apartments, which are commonly seen in tropical developing countries, suffer from poor cross-ventilation, particularly on the leeward side of the buildings. This study aims to parametrically evaluate closed-vertical void configurations to improve the ventilation performance of the double-loaded apartment building using the validated CFD models. The configurations include the aspect ratio of the void, pilotis size and fin size with various wind directions. The results showed that the most influential parameter for enabling natural ventilation by augmenting pressure coefficient differences on the windward and leeward sides of the building was the fin size, followed by wind direction and aspect ratio. Wind direction influenced the windward side more than the leeward side, whereas aspect ratio influenced the leeward side over the windward side. It was concluded that the mass flow rates on both sides of the building could be maximised by optimally combining the void's fin size and aspect ratio under the specific prevailing wind directions. These findings would help create sustainable design guidelines for improving natural ventilation by incorporating a closed-vertical void in the mid-rise apartment buildings in the tropics.

1. Introduction

In general, south-facing apartments with single-loaded corridors are commonly seen in the Northern Hemisphere to receive the low-angle winter sun for heating. Meanwhile, solar radiation is often unsolicited in the tropics, and thus building orientation is not necessarily prioritised [1]. As a result, affordable housing entailing mid-to-high-rise apartments in tropical developing countries generally have double-loaded corridors that maximise the total floor areas [2]. It was reported that double-loaded corridor buildings often suffer from poor environmental conditions such as daylighting, thermal comfort, ventilation and indoor air quality [3–7]. Natural ventilation that is inherently zero carbon is often considered an essential solution for creating livable indoor environments in the tropics. Sufficient provision of natural ventilation would lead to better thermal comfort, energy-saving, and health [8–16], specifically in the double-loaded apartments where the occupants living on the leeward side of the buildings experience poor cross-ventilation in the units. It is imperative to find a passive design for double-loaded apartments to improve the ventilation performance even on the leeward side of the buildings.

The present authors, in their previous work, had proposed an alternative building design for double-loaded apartments for effective indoor ventilation performance on the leeward side of buildings [17]. Fig. 1 illustrates the ventilation concept of the proposed alternative building design that incorporates a closed-vertical void. The proposed design has a pilotis and a closed-vertical void with a slit-shaped wind fin attached to the vertical void's edge on the leeward side. The primary idea of the proposed design was to create a positive pressure region inside the closed-vertical void by combining the effects of pilotis and wind fin. As illustrated in Fig. 1, when the wind reaches the external wall of the building, the wind diverges from a stagnation point and some of the winds are directed downwards to the pilotis. Thus, the Venturi effect can happen at the inlet of the pilotis space [18,19]. In the proposed design, while combining the effects of pilotis and wind fin, the air pressure inside the closed-vertical void increases, creating significant air pressure differences between the two sides of the leeward units. As a result, the

* Corresponding author. 1-5-1 Kagamiyama, Higashi-Hiroshima, 739-8529, Hiroshima, Japan.
E-mail address: tetsu@hiroshima-u.ac.jp (T. Kubota).

https://doi.org/10.1016/j.buildenv.2022.108969
Received 5 January 2022; Received in revised form 16 February 2022; Accepted 5 March 2022
Available online 8 March 2022

wind flows from the windward side to the leeward side of the building, as shown in Fig. 1.

The computational fluid dynamics (CFD) models of the proposed building design were validated using the results of a detailed wind tunnel experiment in terms of grid sensitivity and turbulence models in the previous study [17]. Furthermore, we analysed the effects of the proposed design on indoor ventilation performance compared with a typical apartment building with an open-vertical void. The results showed that the closed-vertical void in the proposed design helped increase wind pressure differences on the leeward side of the building, causing better indoor ventilation for both sides of the double-loaded apartment building [17].

Several researches on open-vertical voids analysed the impacts of void configurations on airflow patterns inside the void and the ventilation performance of buildings. Farea et al. [20] conducted wind tunnel experiments and CFD simulations on high-rise building models with various void designs to investigate the effect of horizontal openings in open-vertical voids on the change in the wind flow pattern. The results suggested strong upward flow in the void with a horizontal opening in the midpoint of the building. Muhsin et al. [21,22] examined the effect of an open-vertical void with changes in sizes on air velocity in residential units, suggesting that increasing the void size by 50% will increase natural ventilation performance by 50.88%. However, there are limited studies of natural ventilation performance on apartment buildings with a closed-vertical void.

It has been reported that wind flow patterns inside the open-vertical voids are strongly influenced by aspect ratios (e.g., height-to-width ratio) [22–24] and incident wind directions [25,26]. These changes in wind flow patterns were also observed in urban street canyons [27]. Oke et al. [28] demonstrated that wind flow patterns in the urban street canyons have three flow regimes: isolated roughness flow, wake interference flow, and skimming flow when parameterized by the aspect ratio. This study hypothesized that the wind flow patterns in the proposed closed-vertical voids will depend on the configurations, particularly the aspect ratio, and may divide into some flow regimes like those for open-voids or urban street canyons.

A building comprises multiple design parameters that enhance the overall building utility [29]. Hence, parametric studies aid in investigating the impact of building design on natural ventilation in and around buildings at various levels, ranging from urban context [25,30–32], site planning [33–37], pedestrian comfort [38–40], building features (e.g., balconies, atrium and windcatcher) [9,41–45] and indoor natural ventilation [45–48]. Sensitivity analysis (SA) helps to identify the contribution of a specific design parameter on the performance of the building while quantifying the uncertainties [29]. SA methods are classified into screening, local and global sensitivity [49]. The local sensitivity method is based on one parameter at a time (OAT) approach, where the calculation of output dependency is based on the variation of one design parameter, while other design parameters are kept constant [50–52]. Although the local sensitivity approach is limited to the effect of a single parameter without considering the interaction effects, it is computationally efficient [53]. Hence, this study uses the local sensitivity to show the effect of design parameters on natural ventilation in a double-loaded closed-void building [54].

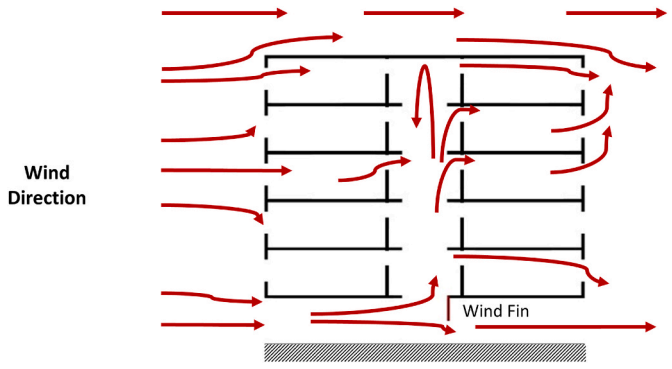

Fig. 1. Natural ventilation concept of the proposed apartment building with a closed-vertical void.

The present study aims to scientifically conduct a parametric evaluation of different design configurations of the closed-vertical void in a double-loaded apartment for improving ventilation performance on the leeward units of the building design. The study's novelty is three folds: First, with the help of CFD simulations, it reveals the detailed wind flow patterns in and around the closed-vertical void of the double-loaded apartment buildings, considering the changes in design configurations. Second, it helps identify the sensitivity of each structural parameter (aspect ratio of the void, pilotis size and fin size under various wind directions) on wind pressure differences across the building. Third, it provides essential design guidelines for future affordable housing, incorporating a closed-vertical void into double-loaded apartment buildings. In this study, CFD simulations using the 3D Reynolds averaged Navier-Stokes (RANS) k-ϵ turbulence model are performed to analyse the natural ventilation performance due to change in parameters such as (i) aspect ratio of the void, (ii) wind direction from perpendicular to parallel to the building façade, (iii) size of the wind fin from no fin to pilotis size fin, and (iv) increase in pilotis size. Grid sensitivity analysis is carried out to check the mesh quality for CFD simulations and the results have been validated with the help of measurements from wind tunnel experiments. Localised sensitivity analysis is conducted to calculate the dependency of the parameters. Finally, the mass flow rates (MFR) are calculated using the orifice equation for representative units on windward and leeward sides of the building.

In this paper, Section 2 describes computational settings of the CFD simulation, comprising the building model and simulation cases, details of the computational domain, CFD solver settings with inflow conditions and calculation of mass flow rates. Section 3 presents the results of a grid sensitivity analysis and validation for the CFD model with the help of experimental data collected from the wind tunnel experiment. The results from the parametric study with varying void size, wind direction and wind fin size are presented in Section 4. Section 5 presents the sensitivity analysis results of the building design elements for pressure changes on the windward and leeward sides of the building. Furthermore, the MFRs in the units have been compared in Section 6. The concluding remarks with the limitations and future scope are described in Section 7.

2. CFD simulation settings

2.1. Building model and simulation cases

A prevalent mid-rise 5-storey apartment building with a closed-vertical void was used as a test case to parametrically study the effect of design elements on the natural ventilation performance (see Fig. 2). A base simulation model was designed at a scale of 1:75 with 0.6 m in length (L), 0.25 m in height (H) and 0.108 m in width (W) for windward and leeward units, which represent 45 m (L), 18.75 m (H) and 8.1 m (W) in full scale. This reduced-scale was determined based on the wind tunnel experiment previously conducted by the present authors [17]. Several cases were then developed computationally that had varied pilotis height (P), fin size (F), and void width (W). The unit spaces of windward and leeward sides were simplified as solid volume spaces of 0.014 m^3 to reduce the model complexity. Wind pressure data were computed for the exterior and interior walls of the building's windward and leeward sides (Walls 1–4). Wind velocities were measured on Lines A-D (see Fig. 2). Lines A and C are located at 0.14 m from the centre of the void, whereas Line D is placed at the height of 0.01 m from the ground level.

To find the optimum ventilation performance of the proposed double-loaded closed-vertical void design, 36 cases were simulated in

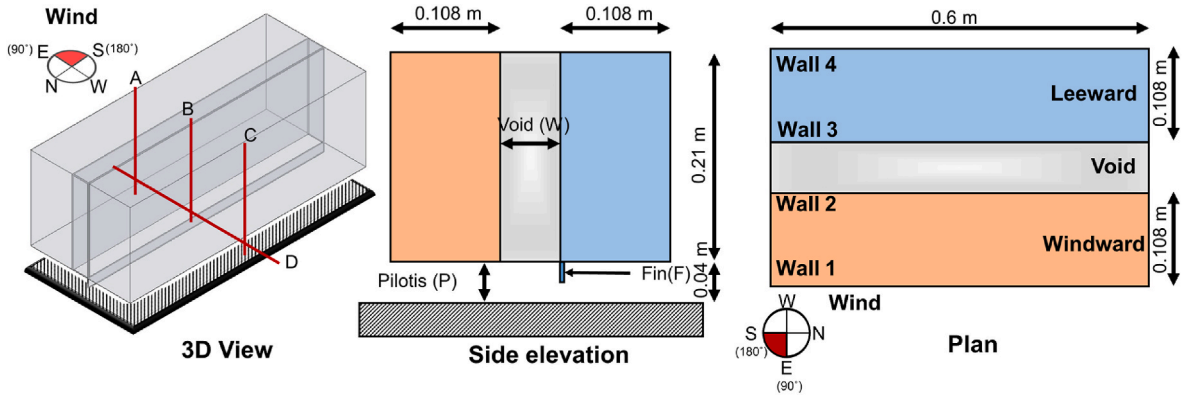

Fig. 2. Simulation model with measuring points for wind velocity (red lines). (a) 3D perspective, (b) Side elevation, (c) Plan. Wind pressures on Walls 1–4 were also measured. (For interpretation of the references to colour in this figure legend, the reader is referred to the Web version of this article.)

four separate sub-studies (Study 1–4) where the void width (W), fin height (F), pilotis height (P) and wind direction were varied (see Table 1). The building design elements were computed as dimensionless ratios using the following equations.

$$Aspect\ ratio = W/H \tag{1}$$

$$Pilotis\ size = P/H \tag{2}$$

$$Fin\ size = F/P \tag{3}$$

where H is the building height, W is the void width, F is the fin height and P is the pilotis height. In each simulation, the size of a building element was varied while the rest of the elements were kept constant to study the sensitivity of the building element. In Study 1, the aspect ratio *(W/H)* of the vertical void was varied between 0.05 and 2; in Study 2, the wind direction was varied between 90° and 180°. Study 3 included cases with and without fins with pilotis size (*P/H*) varying between 0.12 and 0.24. Study 4 included the effect of the wind fin size (*F/P*) while the other parameters were kept constant.

2.2. Computational geometry, domain and grid

Fig. 3 shows the computational domain, which was made according to the AIJ guidelines [55]. The dimension of the largest computational domain is 5.72 m (D), 3.1 m (W) and 1.5 m (H). The resulting blockage ratio is 2.7%, which is below the maximum value recommended by the AIJ guidelines of 3% [55]. Two domains at a distance of 0.025 m and 0.13 m from the building were constructed to create finer mesh sizes around the building.

The vertical profile of U was considered as the power-law shape with an exponent of 0.25:

$$U(z) \Big/ U_H = (z/H)^{0.25} \tag{4}$$

The inlet boundary conditions for U and k were determined based on the measured data from the wind tunnel experiment conducted by Kumar et al. [17]. The turbulent dissipation rate (ϵ) distribution was calculated as recommended by Tominaga et al. [55].

$$\varepsilon(z) = C_{\mu}^{\frac{1}{2}} k(z) \frac{U_H}{H} \alpha \left(\frac{z}{H}\right)^{\alpha-1} \tag{5}$$

where C_μ is the model constant 0.09 and α is the power-law exponent, which is 0.25. k is turbulent kinetic energy. Fig. 4 shows the vertical profiles of inlet boundary conditions of wind velocity (Fig. 4a), turbulent kinetic energy (Fig. 4b) and turbulence dissipation rate (Fig. 4c).

The standard wall function was used as the boundary condition for the building and bottom surface of the computational domain [56]. The symmetric boundary condition was applied to the domain ceiling and sides, suggesting that all variables at these boundaries had zero normal velocity and zero gradients [57,58]. The outflow boundary condition was assumed to be zero static pressure.

This study advances on the previous research by the authors [17], where a systematic validation, including grid sensitivity and turbulence models, was performed using the results of the wind tunnel experiment. Here, to ensure the required blockage ratio, the computational domain size was increased from the previous study [17]. The grid sensitivity analysis considering three mesh sizes were computed to maintain robustness of the results. Meshing was constructed using a cut-cell mesh generated by ANSYS Mesh. The cut-cell mesh reduced the computational time as it is computationally fast and memory lean [59]. In this analysis, the mesh sizes were determined by refining and coarsening the primary medium grid by a factor of $\sqrt{2}$ in each direction.

Table 2 summarises the details of the mesh sizes for respective domains and the total number of elements. In the coarse mesh, the maximum length of mesh size was kept at 0.3 m, which was reduced to 0.0375 m and 0.0075 m near the building for Domain 2 and 3, respectively (see Fig. 3). The sides and building walls were set at 0.075 m and 0.03 m, respectively. An inflation layer was created around the building with 0.0005 m and at the bottom with 0.001 m width. Fig. 3b shows the grid distribution inside the domain for the medium mesh. In the medium mesh, the spatial grid resolution was increased to 0.025 m in Domain 2, which was further increased to 0.005 m around the building in Domain 3 (Fig. 3c). In Domain 3, the resolution was increased around the boundary plane of the building to 0.0018 m (Fig. 3d), which was increased further around the building with an inflation layer of 0.0005

Table 1
Details of simulation cases.

Study	Aspect ratio *(W/H)* [−]	Wind direction [°]	Pilotis size *(P/H)* [−]	Fin size *(F/P)* [−]	Parameter considered	Reference to illustrations
1	**0.05–2**	90	0.16	0.5	Aspect ratio of void *(W/H)*: 0.05–2	Fig. 9
2	0.15	**90–180**	0.16	0.5	Wind direction: 90°–180°	Fig. 10
3	0.15	90	**0.12–0.24**	0,1	Pilotis size *(P/H)* with no and full-size fin: 0.12–0.24	Fig. 11c and d
4	0.15	90	0.16	**0 to 1**	Fin size *(F/P)*: 0, 0.25, 0.5, 0.75 and 1	Fig. 11a and b

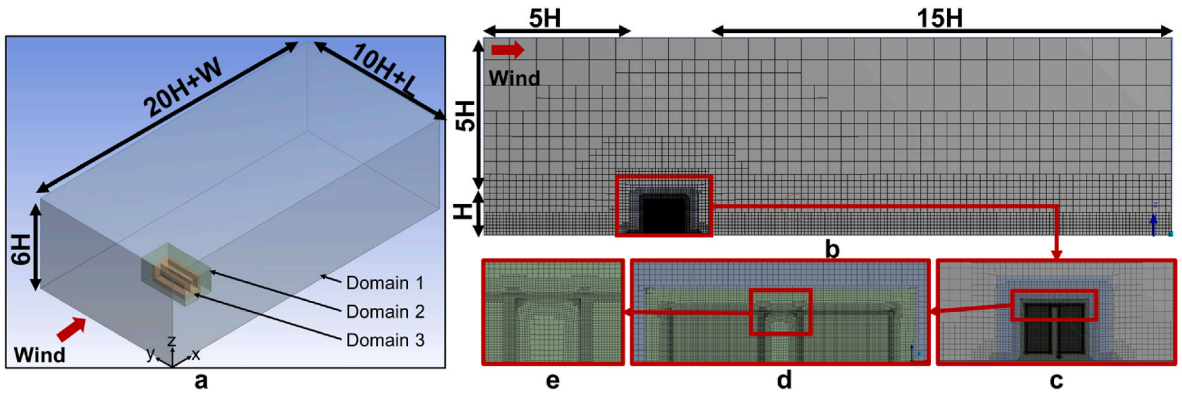

Fig. 3. (a) Computational domain, grid distribution for (b) the entire computational domain, (c) at the building level, (d) upper part of the building and (e) upper part of the vertical void.

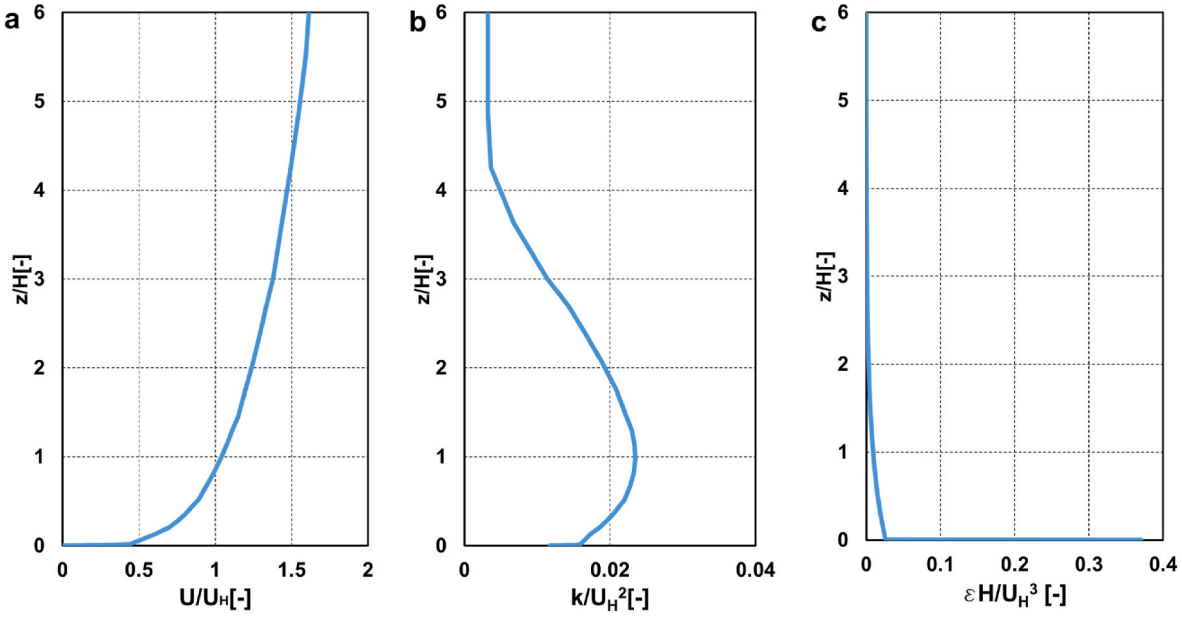

Fig. 4. Vertical profiles of dimensionless U, k and ϵ at the inlet of the domain.

Table 2
Element sizes used for coarse, medium and fine mesh.

	Coarse [m]	Medium [m]	Fine [m]
Domain 1	0.3	0.2	0.135
Domain 2	0.0375	0.025	0.0135
Domain 3	0.0075	0.005	0.002
Bottom	0.03	0.02	0.01
Sides	0.075	0.05	0.035
Building	0.003	0.0018	0.001
Total elements	2,214,258	6,652,135	16,957,971

m (Fig. 3e). In the fine mesh, the maximum mesh length was set at 0.135 m, whereas Domains 2 and 3 were 0.0135 m and 0.002 m, respectively. The mesh size around the building and at the bottom was set at 0.001 m and 0.01 m, respectively, which results in total numbers of mesh elements of 221,425, 6,652,135 and 16,957,971 for the coarse, medium and fine meshes. Fig. 5 shows the grid configuration of the same area in the vertical void, with the three mesh types: coarse, medium and fine.

2.3. CFD solver settings

The finite volume approach in the ANSYS Fluent 18 was used to solve the governing equations for mass and momentum. In this study, the RANS Realizable k-ϵ [60] turbulence model was used based on the results of the previous systematic validation study [17]. The advection terms for all the transport equations were discretized using a second-order upwind scheme and the pressure interpolation was kept at second order. The semi-implicit method for pressure-linked equations (SIMPLE) algorithm was used for pressure velocity coupling of the RANS simulation model. Convergence was assumed to be obtained when all the scaled residuals leveled off and reached the minimum of 10^{-6} for x, y, z momentum, 10^{-4} for k, ϵ and continuity. All simulations were conducted on the Dell Precision Tower 7810 with Intel® Xeon® CPU E5-2620 and 32 GB of system memory.

The results of the parametric study were obtained in the form of wind velocity ratio (WVR) and pressure coefficient (C_p), which were computed as follows:

$$WVR = \frac{V_M}{U_H} \tag{6}$$

$$C_p = \frac{(P - P_0)}{0.5\rho\ U_H^{\ 2}} \tag{7}$$

where V_M is the velocity magnitude, U_H is the free flow velocity

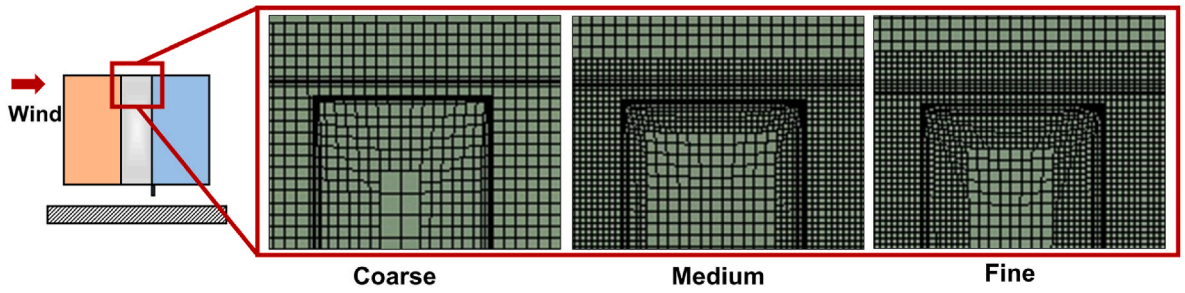

Fig. 5. Grid distribution in coarse, medium and fine grids.

magnitude at the building height, 3.95 m/s, P is the pressure at the surface, P_0 is the static reference pressure, and $\rho = 1.225$ kg/m^3 is the air density.

2.4. Mass flow rate calculation method

Ventilation performance of the building was evaluated by assessing the mass flow rates (MFR) in representative units on each floor (Fig. 6). Since the simulation model was simplified as solid volume spaces as explained before, standard-size window openings were assumed on the windward and leeward sides of units at the middle, left and right building row. The opening size was assumed as 0.02 m × 0.02 m, which is 1.5 m × 1.5 m in full scale, on all four walls for each floor. Average wind pressures over all the 60 surfaces (assumed window openings) were then calculated from the CFD simulation results.

Based on the obtained average wind pressures of windward and leeward sides of units, the MFRs in the respective units were calculated using the following orifice equation (Eq. (8)). The equation is formed on the principle that the turbulent unidirectional mass flow rate through any sharp-edged opening is proportional to its cross-sectional area and is also a function of pressure drop across the opening [61], which is normalised as (q_0) using Eq. (9).

$$q_{unit} = c_d A_w \sqrt{\frac{2\Delta \overline{P_W}}{\rho}} \tag{8}$$

$$q_0 = \frac{q_{unit}}{U_H A_w} \tag{9}$$

where c_d is dimensionless discharge coefficient, which is assumed to be a fixed value of 0.7 [62], A_w is the opening area, ρ is the air density, U_H is the free flow velocity magnitude at the building height, 3.95 m/s, and $\Delta \overline{P_W}$ is the difference of the averaged static pressures between the windward and leeward assumed windows of each building unit.

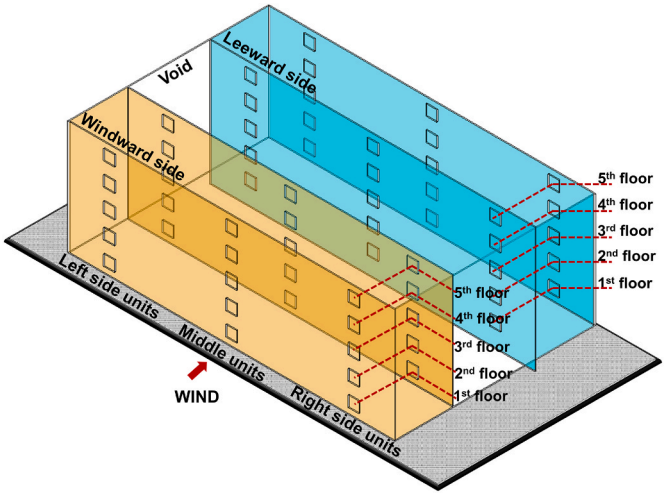

Fig. 6. Location of assumed windows for measuring mass flow rates of the units.

3. Verification and validation of CFD model

3.1. Grid sensitivity analysis

The RANS Realizable k-ϵ turbulence model with three grid sizes, coarse, medium and fine mesh was used to conduct the grid sensitivity analysis. Roache [63] suggested that the grid convergence index (GCI) (Eq. (10)) quantify the inaccuracy in outcomes for different mesh sizes:

$$\mathrm{GCI}_{\mathrm{Medium}} = \mathrm{F_s}\left|\frac{r^q[(UMedium - U_{Fine})/U_H}{1 - r^p}\right| \tag{10}$$

where F_s is the safety factor ($F_s = 1.25$ when three or more grids are considered) [63], r is the linear grid refinement factor ($r = \sqrt{2}$), q is the formal order of accuracy, which is assigned as a value of 2 due to second-order discretisation schemes used in simulations, U_{Medium} and U_{Fine} are the velocities obtained in the medium and fine mesh respectively and U_H is the time-averaged wind velocity at the height of the building. With modifications in grid sizes from medium to fine or coarse, GCI enables an evaluation of the inaccuracy in the simulation results.

Table 3 shows the average GCI for the three mesh types for wind velocity on Lines A-D. Fig. 7 presents the wind velocity profiles on Lines A-D for medium grid size and absolute deviations between the coarse and fine mesh from the medium mesh. The error percentages are mentioned in Table 3. As shown in Fig. 7, Line A depicts a slight deviation from pilotis top to mid building height and the cumulative error is from 0.93% to 1.41%. Line B has the error at the junction of pilotis to the void in which the cumulative error is from 0.25% to 0.66%. Line C, which is on the leeward side of the building, has an error at the pilotis level, particularly the mid-section of the building, with the maximum cumulative error of 1.87%. Line D, which is a horizontal line through the pilotis of the building at the height of 0.001 m, has deviations before the building location and after the building in the wake region with the maximum cumulative error of 2.19%. This is mainly because Line D lies in the induced flow region by the outgoing jet from the leeward units. It can be concluded that the results have a low grid sensitivity and any of the meshes will provide appropriate simulation results. Hence, the medium mesh was used for all further RANS simulations.

3.2. CFD model validation

The wind tunnel at Niigata Institute of Technology (NIT) in Japan

Table 3
Percentage of GCI values among different mesh sizes for wind velocity (WS).

GCI values	WV Line A	WV Line B	WV Line C	WV Line D
Coarse-Medium	0.93%	0.66%	0.79%	1.75%
Fine-Medium	1.41%	0.25%	1.87%	2.19%

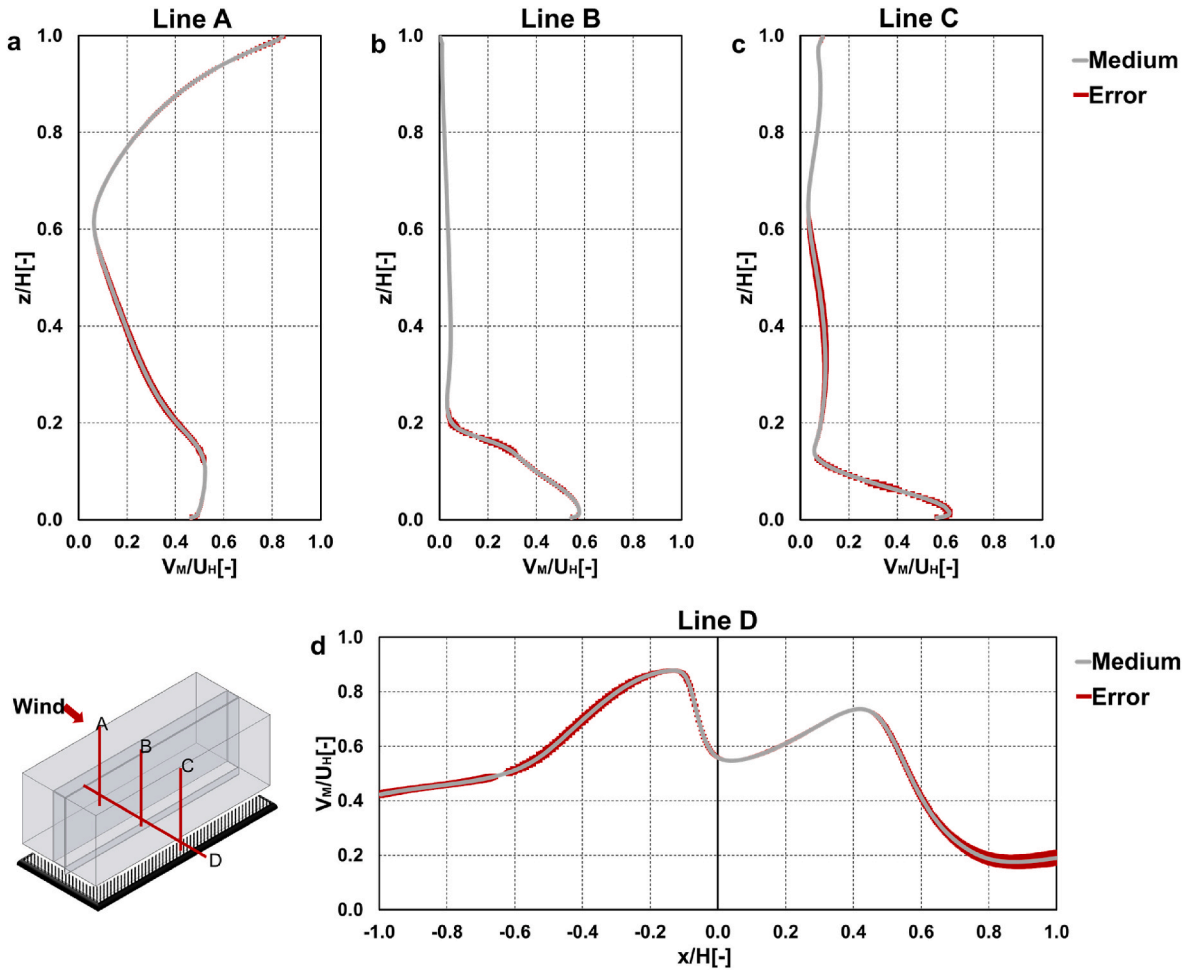

Fig. 7. Dimensionless wind velocity profiles for medium-mesh with error deviations from fine and coarse mesh at vertical (a) Line A, (b) Line B, (c) Line C and horizontal (d) Line D.

was used to carry out experimental measurements [64–66]. The 13 m long atmospheric boundary layer wind tunnel has a 1.8 m × 1.8 m cross-section. The wind tunnel settings have been specified in the previous work [17]. Wind pressure and wind speed were measured using the multi-point transducer (Kyowa Electronic Instruments; F94-2206) [17,67–69] and a thermistor anemometer probe (AS201-7, Shibaura Electronics) [17,66], respectively.

Fig. 8 shows the comparison of experimental measurements to those of CFD simulation using the RANS Realizable k-ϵ turbulence model. The CFD simulation was conducted using the wind tunnel size as the base to ensure similar domain and boundary conditions with the dimensions of 5.3 m (D), 1.8 m (W) and 1.8 m (H). The results were compared with those with an increased computational domain of which a lateral distance was *5H* on both sides. The results indicated that the lateral distance between the model and the wind tunnel sidewalls had no significant effect on the velocity and pressure distributions around the model.

The details of the experimental building model used for wind tunnel experiments is shown in Fig. 8, in which four vertical rows of units were repeated on each floor and experimental data were collected. Fig. 8 indicates two sections showing the measuring locations for the wind pressure on Lines E-H, which lie on the walls of the building. The wind speed was measured on Lines I, J in the void's centre. The measurements were carried out in the centre of each floor. The results show the vertical distribution of wind pressure (C_p) on Lines E-H and wind velocity (V_M/U_H) on Lines I, J for the experiments and CFD simulations (Fig. 8). Overall, the results of C_p indicate little differences among the pressure on the walls for the simulation and experimental measurements. The V_M/U_H measurements in the experiment and simulation also varied slightly. The Pearson's product-moment correlation coefficient (R) [70] was calculated for the experimental and CFD measurements, and the R-values for wind velocity (V_M/U_H) and wind pressure (C_p) showed a reasonable correlation with values 0.988 and 0.915, respectively.

4. Parametric study

4.1. Void aspect ratio

The impact of aspect ratio of the void *(W/H)* was investigated by changing width of the voids under the wind direction of 90° with the fixed pilotis and fin sizes (i.e., Study 1 in Table 1). Fig. 9a illustrates the contour of wind pressure (C_p), wind velocity (V_M/U_H) and streamlines parallel to the wind direction (90°) at the vertical central plane for the representative aspect ratios of 0.15, 0.4, 0.8 and 1.5 *W/H*. As shown, wind velocity (V_M/U_H) is significantly high at the inlets of the pilotis for all the cases regardless of the aspect ratio. This increase is primarily due to the Venturi effect, which was analysed in the previous study [17]. When the approach flow is perpendicular (90°) to the void, the increased winds in the pilotis are directed upwards due to the wind fins and create an isolated vortex inside the void. The volume of inflows should be almost the same for all the cases, while the volume of the void (i.e., reservoir) changes along with its aspect ratio. Hence, when the aspect ratio is small such as 0.15 *W/H*, the higher dynamic pressure is converted into the static pressure inside the void due to the flow resistance

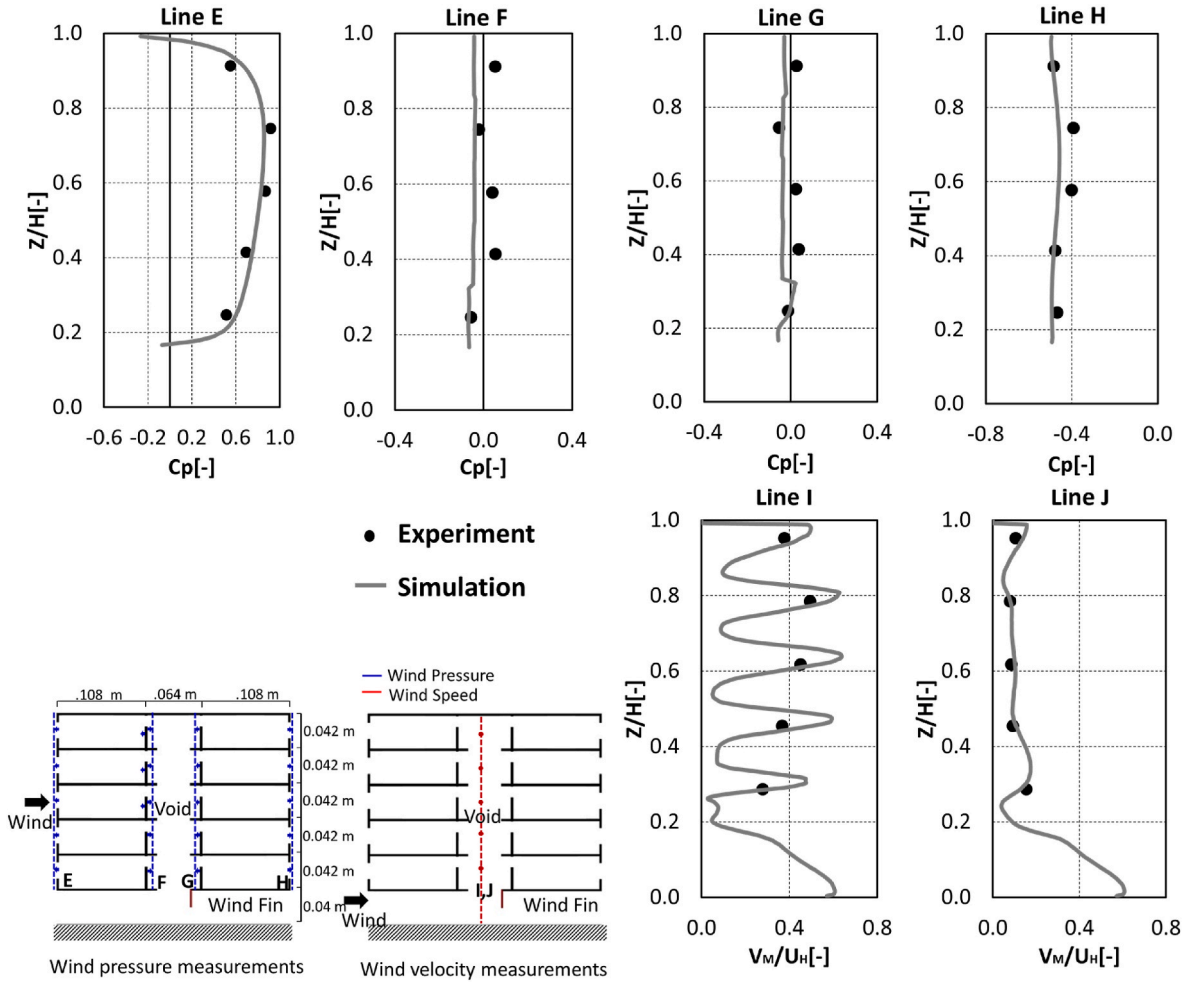

Fig. 8. Vertical profiles of dimensionless wind velocity, wind pressure with simulation and experimental measurements.

mainly caused by its closed rooftop. The dynamic pressure decreases with the increase in aspect ratio, and thus the converted static pressure inside the void, C_p, decreases accordingly. The isolated vortex is confined by the void until the aspect ratio of around 0.8 *W/H*. During this regime, $W/H < 0.8$, the size of the confined vortex gradually increases with the increase in aspect ratio. After the above threshold point (i.e., around 0.8 *W/H*), the size of the vortex decreases as the aspect ratio increases, reducing C_p inside the void to almost the same level of the leeward wake region. The above vortexes in the closed-vertical voids behave like the skimming flow for urban street canyons [28]. In the case of urban canyons or open-vertical voids, the wind speeds inside the voids or ventilation rates of the buildings were generally increased as the aspect ratio *(W/H)* increased because of the increase in inflow volume to the voids [27,28], which is an important difference from the present results.

As depicted in Fig. 9a, the centre of the vortex is situated near the inlet of the void when the aspect ratio is 0.15 *W/H*, but the centre moves upwards with 0.4 *W/H*, further moves to the left for 0.8 *W/H* and to the upper part of the void with 1.5 *W/H*. Although V_M/U_H at the centre of the vortex is less than 0.2 for all the cases, V_M/U_H around the sides gradually increases with the increase in aspect ratio. The C_p inside the void is generally positive with values of less than 0.2 when the aspect ratio is 0.15 *W/H*. However, it reduces and becomes negative as the aspect ratio increases further. Overall, C_p on the external wall of the windward side (Wall 1) is similar for all the cases. C_p on the void walls (Walls 2 and 3) decreases with the increase in aspect ratio. The distribution of C_p values is almost the same between Wall 2 and 3 for each case, where C_p is slightly higher near the roof and pilotis than those in the middle of the walls. C_p on Wall 4 is almost equal to those on Walls 2 and 3 when the aspect ratio reaches 1.5 *W/H*. This means that a significant difference of C_p on the leeward side of the building cannot be expected when the aspect ratio exceeds around 1.5 *W/H*.

Fig. 9b shows the boxplots of wind pressure (C_p) distribution on Walls 1–4 with the change of aspect ratios (*W/H*) from 0.05 to 2 under the wind direction of 90°. C_p on Wall 1 is similar in all the cases, with an average of 0.7. As described before, C_p on the void walls (Walls 2 and 3) are similar and their C_p values decrease with the increase in aspect ratio, particularly until 0.7 *W/H*. Their average C_p is around 0.17 when the aspect ratio is 0.05 *W/H*, but the average values turn negative when the aspect ratio exceeds 0.2 *W/H*. The reduction of average C_p values becomes slower when the aspect ratio is increased to 0.7 *W/H* and more. C_p on the external wall of the leeward side (Wall 4) is negative in all the cases. Meanwhile, the average C_p value on Wall 4 gradually increases with the increase in aspect ratio from −0.4 to −0.3 and the average value becomes almost equivalent to those of internal walls of the void (Walls 2 and 3) when the aspect ratio becomes 2 *W/H*.

The difference of C_p between Walls 1 and 2, which affects the ventilation performance of the windward side of the building, varies depending on the position of the units as there is a relatively large distribution in C_p on Wall 1. Nevertheless, the said difference of C_p increases with the increase in aspect ratio. On the other hand, the corresponding difference of C_p for the leeward side of the building (between Walls 3 and 4) is the maximum when the aspect ratio is the smallest (i.e., 0.05 *W/H*) and reduces with the increase in aspect ratio.

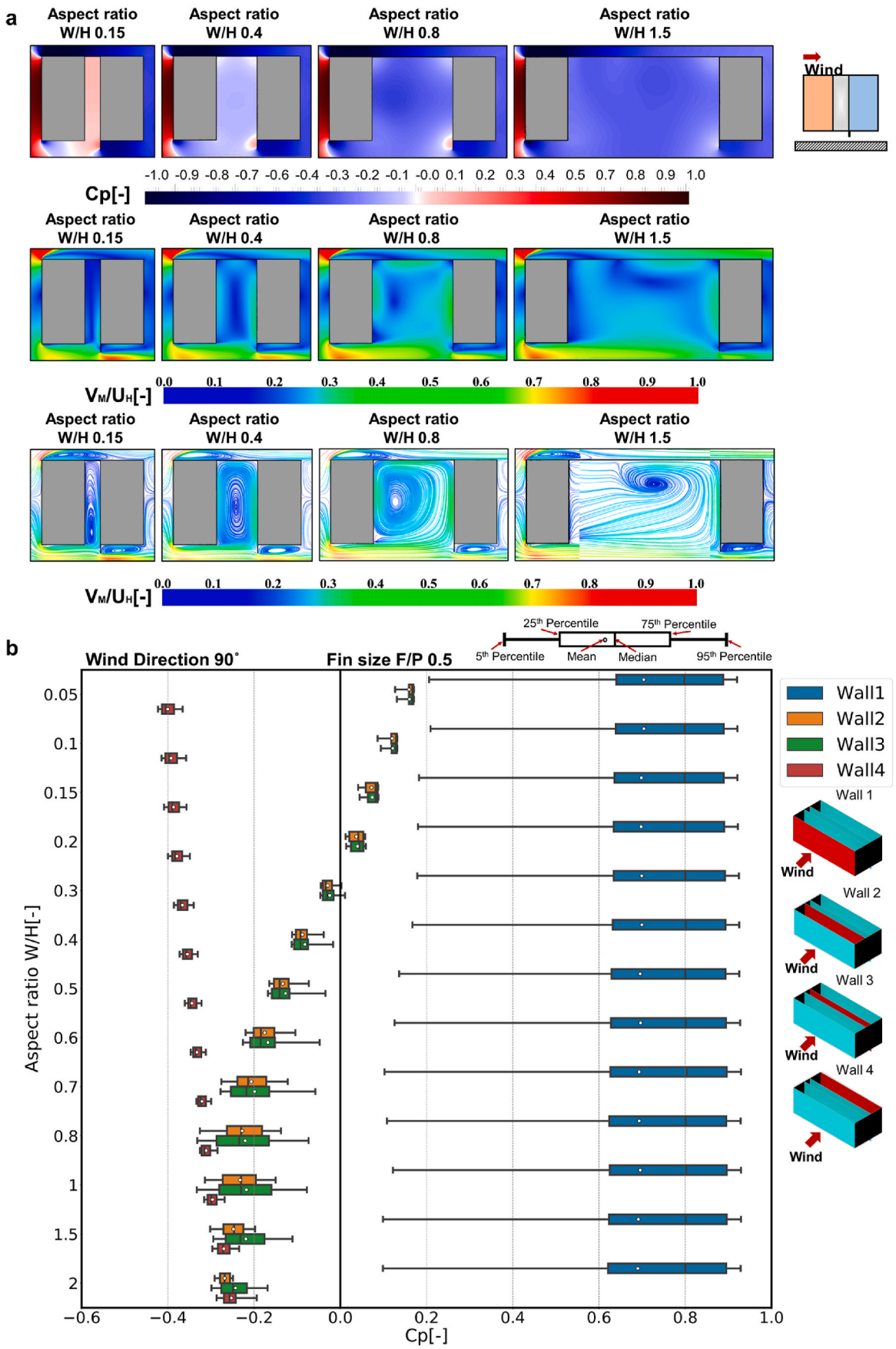

Fig. 9. (a) Dimensionless wind velocity, streamlines and wind pressure in section; (b) Boxplots of wind pressure on the walls with the various aspect ratios.

To ensure adequate natural ventilation conditions in both windward and leeward sides of the building, the C_p differences between Walls 1 and 2, as well as Walls 3 and 4, should be maximised simultaneously. The C_p differences on the windward and leeward sides are maximised between aspect ratios of 0.1 and 0.15 *W/H*, tending towards 0.15. Therefore, the aspect ratio of 0.15 is recommended as the C_p differences of the windward and leeward sides are 0.6 and 0.5, respectively. Further simulations with other parameters were conducted with an aspect ratio of 0.15 *W/H* in the following sections.

4.2. Wind direction

The impact of the change in wind direction was investigated with an aspect ratio *(W/H)* of 0.15. The wind direction was changed from 90° (Perpendicular to the front façade) to 180° (parallel to the façade) in 10° steps with fixed pilotis and fin sizes (i.e., Study 2 in Table 1). Fig. 10a illustrates the contour of wind pressure (C_p), wind velocity (V_M/U_H) and streamlines at the vertical central plane with an aspect ratio of 0.15 under the wind directions of 110°, 130°, 160° and 180° (the results of 90° were shown in the previous section). The wind velocity (V_M/U_H) of inflows near the front façade increases with the increase in wind direction until 160°, resulting in the reduction of C_p on the windward façade. Nevertheless, the change of V_M/U_H in inflows does not significantly affect V_M/U_H near the inlets of the pilotis at least until 160° and the increased V_M/U_H due to the Venturi effect can be observed. The isolated vortex is formed inside the void until 130°, but when the wind direction exceeds 130°, the vortex cannot be observed at the vertical plane. Instead, a larger and decentralised vortex is formed, parallel to the oblique wind direction at the different axis in the void (nearly parallel to the windward wall). Like those in urban street canyons [28], when the wind direction became 160°, helical flows were observed inside the void and from 160° to 180°, wind speeds inside the void increased due to the channeling effect. Consequently, C_p in the void is positive values (0.05–0.3) for most areas for 110°and 130°, whereas it is negative (−0.5 to −0.2) for 160° and 180°. The C_p contours for 110° and 130° are similar to that of 90° (see Fig. 9a). Overall, a clear difference of C_p between Walls 1 and 2 can be seen for 110° and 130°, but it is largely reduced for 160° and almost none for 180°. The C_p difference on the windward and leeward sides decreases steadily as the incident wind direction varies from 90° to 180°. Similar results were obtained by CFD simulations [26] and wind tunnel experiments [71].

Fig. 10b shows the boxplots of wind pressure (C_p) distribution on Walls 1–4 with the change of wind direction from 90° to 180°. C_p on Wall 1 gradually decreases along with the increase in deviation as the wind direction increases until 130° and the reduction of C_p becomes faster together with the deviation from 140° to 180°. The average C_p becomes negative value from 170° to 180°. When the wind direction is 180°, the distribution of C_p on Wall 1 (windward) becomes almost the same as that of Wall 4 (leeward). As before, the distributions of C_p on Walls 2 and 3 have a similar pattern for all the cases and on average, the C_p values are positive (0.05–0.07) until 140°. On the other hand, the average C_p on Wall 4 decreases along with the slight increase in deviation until 140°, but it begins increasing from 150° to 180°. This is primarily due to the change of the wind flow patterns around the building. It was found from the CFD results that until 140°, the front façade (Wall 1) receives more wind volume, but from 150°, higher wind volume is received by the sidewall.

4.3. Fin and pilotis size

The impact of the change in fin size *(F/P)* and pilotis size *(P/H)* was investigated based on the aspect ratio *(W/H)* of 0.15 and wind direction of 90° (i.e., Study 3–4 in Table 1). The fin size *(F/P)* was increased by every 0.25 until 1 (Fig. 11a and b), whereas the pilotis size *(P/H)* was increased by 0.04 from 0.12 to 0.24 with or without the wind fin with a size of 1 *F/P* (Fig. 11c and d). Fig. 11a illustrates the contour of wind pressure (C_p), wind velocity (V_M/U_H) and streamlines at the vertical central plane with an aspect ratio of 0.15 and incident wind direction of 90° for various fin sizes, 0, 0.25, 0.5, 0.75 and 1 *F/P*. As shown, V_M/U_H near the inlets of the pilotis gradually reduces with the increase in fin size as the cross-sectional areas of pilotis reduce. The isolated vortices are formed inside the voids except for the no-fin condition, where the counter stacked vortex is observed near the roof. The V_M/U_H inside the void is averagely higher when the fin's size is larger, resulting in an increase in wind pressure inside the void. C_p in the void and pilotis of the windward side gradually becomes positive from the fin size of 0.5 *F/P*. As expected, C_p on Walls 2 and 3 (inside the voids) cannot be increased compared with that of Wall 4 (leeward side) without using the wind fin. While the distributions of C_p on Walls 1 and 4 are almost uniform regardless of the change of the fin size, C_p values on Walls 2 and 3 increase with the increase in fin size, as discussed before. Cruz-Salas et al. [72] and Montazeri et al. [73] used various wind fin designs to direct the airflow in and out of the units from the rooftop of open-vertical voids. The above studies suggested that the incident wind direction is an essential feature for improving airflow in the units.

Fig. 11b shows the boxplots of wind pressure (C_p) distribution on Walls 1–4 with the change of the fin size *(F/P)*. As shown, the average C_p on Wall 1 slightly reduces with the increase in fin size, whereas the corresponding C_p on Wall 4 also slightly reduces simultaneously. As described before, the average C_p on Walls 2 and 3 significantly increases with fin size. Unlike the aspect ratio, as the fin size increases, the difference of C_p for the windward side of the building (between Walls 1 and 2) generally reduces, while the corresponding difference of C_p for the leeward side (between Walls 3 and 4) increases from the fin size of 0.25 *F/P*.

As shown in Fig. 11c and d, the average C_p values gradually increase with the increase in pilotis size for Wall 1 (windward) and Walls 2–3 (inside voids). On Wall 4 (leeward), as the pilotis size increases, the average C_p slightly increases when the wind fin is not attached, whereas the corresponding average C_p slightly reduces when the fin is installed. It can be seen that the impact of the pilotis size on the ventilation performance of the leeward side of the building is generally much smaller than that of the fin size.

5. Sensitivity analysis

Fig. 12 shows the change in the differences of the averaged pressure coefficients ($\Delta\overline{C_p}$) on the windward and leeward sides of the building with changes of input parameters, such as aspect ratio, wind direction, fin size and pilotis size, respectively. As described before, the aspect ratio *(W/H)* is set to be 0.15 except for Fig. 12a, whereas the fin size *(F/P)* is 0.5 except for Fig. 12c. All the cases except for Fig. 12b were analysed under the wind direction of 90°. The differences of the averaged pressure coefficients on the windward (*WW*) and leeward (*LW*) sides of the building ($\Delta\overline{C_{pWW}}$ and $\Delta\overline{C_{pLW}}$) were calculated as follows:

$$\Delta\overline{C_{pWW}} = \overline{C_{pW1}} - \overline{C_{pW2}} \tag{11}$$

$$\Delta\overline{C_{pLW}} = \overline{C_{pW3}} - \overline{C_{pW4}} \tag{12}$$

where $\overline{C_{pW1}}$ to $\overline{C_{pW4}}$ are the averaged pressure coefficients on Walls 1–4, respectively.

As depicted in Fig. 12a, the aspect ratio is particularly influential to $\Delta\overline{C_p}$ values on both sides of the building until 0.8–1 *W/H*. As described before, an isolated vortex was formed inside the void and the size of the vortex gradually increased as the aspect ratio increased until approximately 0.8 *W/H*. $\Delta\overline{C_p}$ values of both sides of the building are equalised around the aspect ratio of 0.15 *W/H*.

The sensitivity profiles of wind direction to $\Delta\overline{C_p}$values vary between the two sides of the building (Fig. 12b). $\Delta\overline{C_{pWW}}$ varies depending on the position of the units, but averagely, it gradually reduces with the

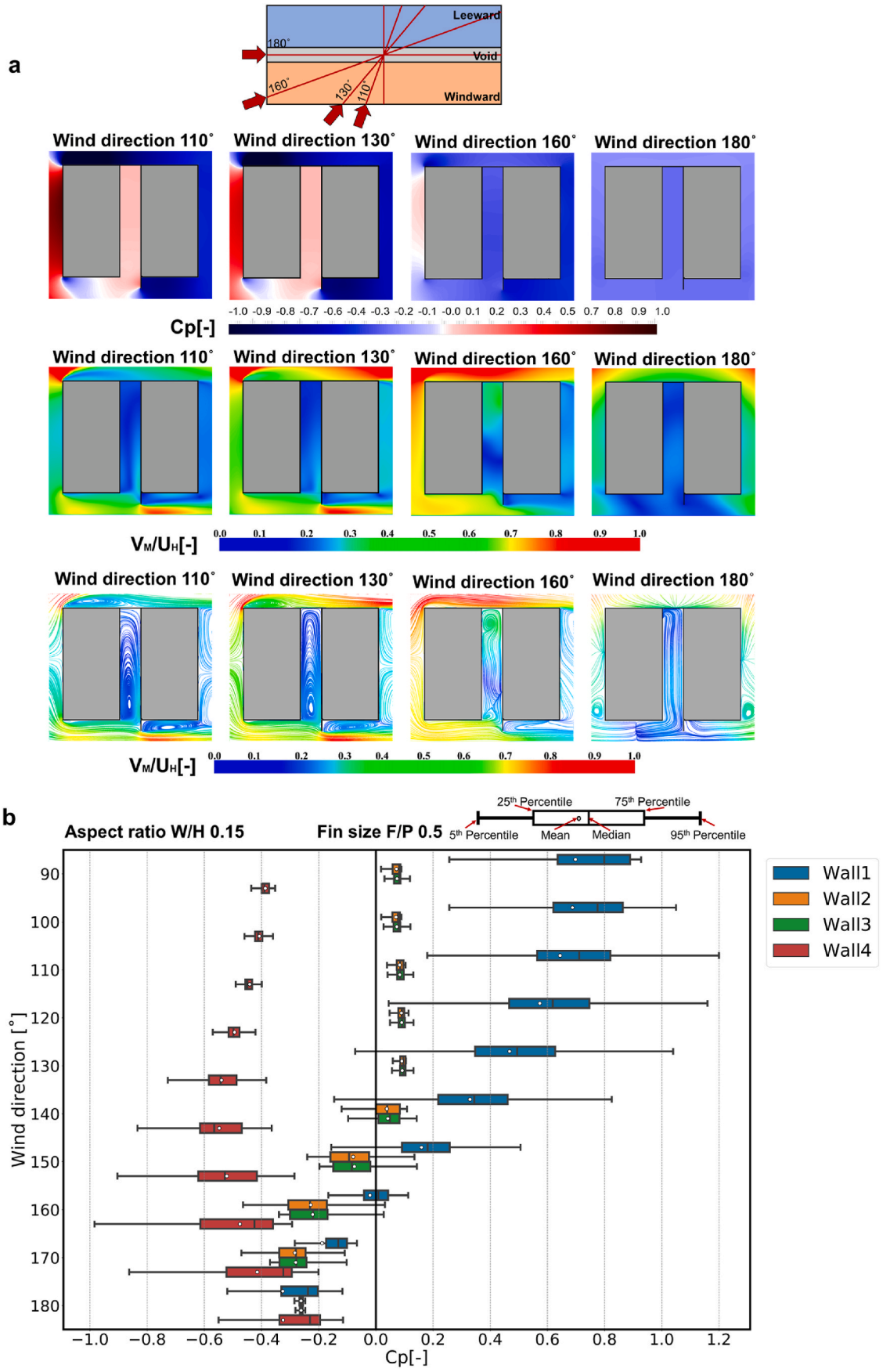

Fig. 10. (a) Dimensionless wind velocity, streamlines and wind pressure in section; (b) Boxplots of wind pressure on the walls with the various wind directions.

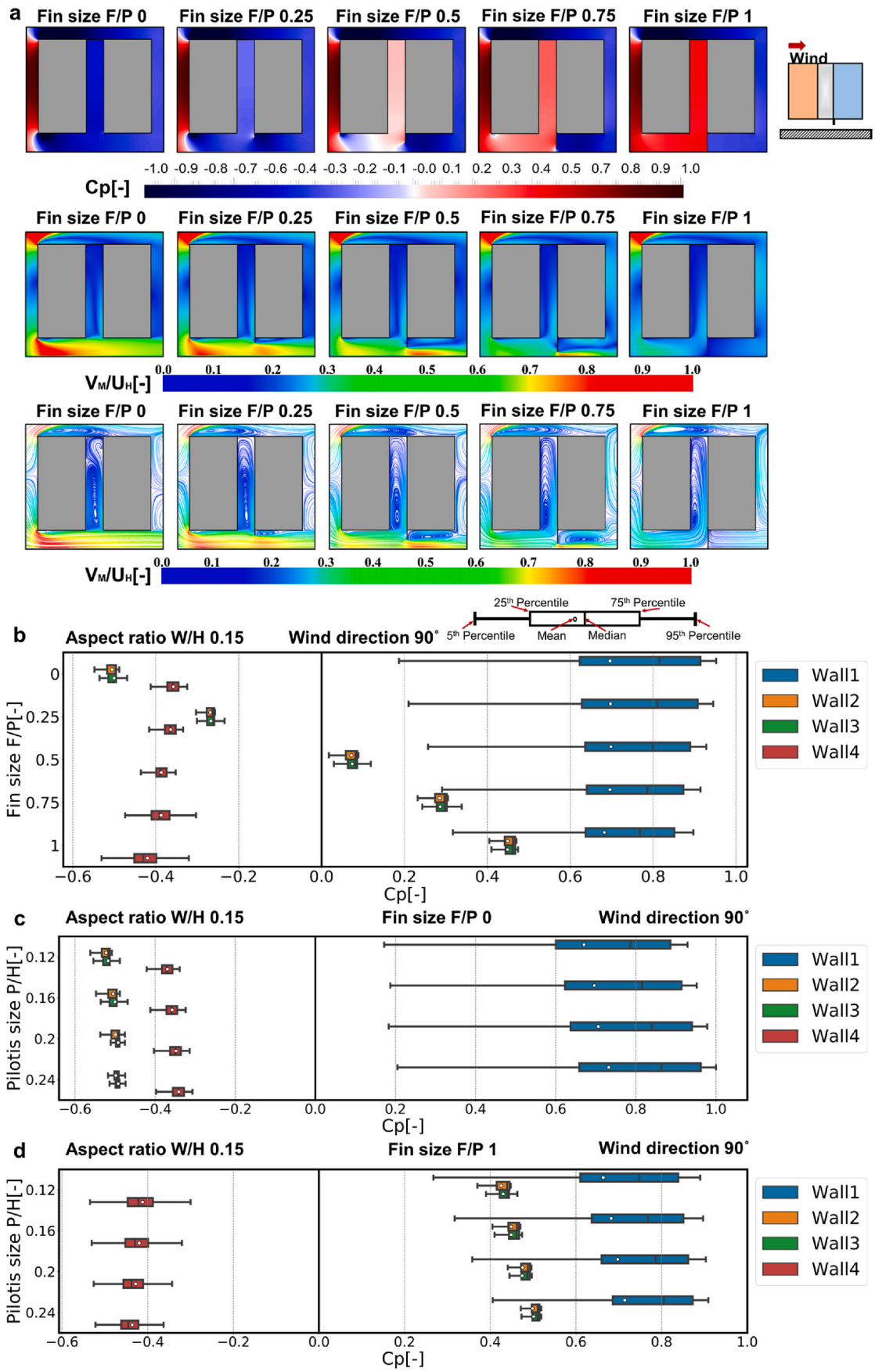

Fig. 11. (a) Dimensionless wind pressure, wind velocity and streamlines of the void section with various fin sizes. Boxplots of wind pressure on the walls with various (b) fin sizes, (c) pilotis sizes without fin and (d) pilotis sizes with fin of 1 F/P.

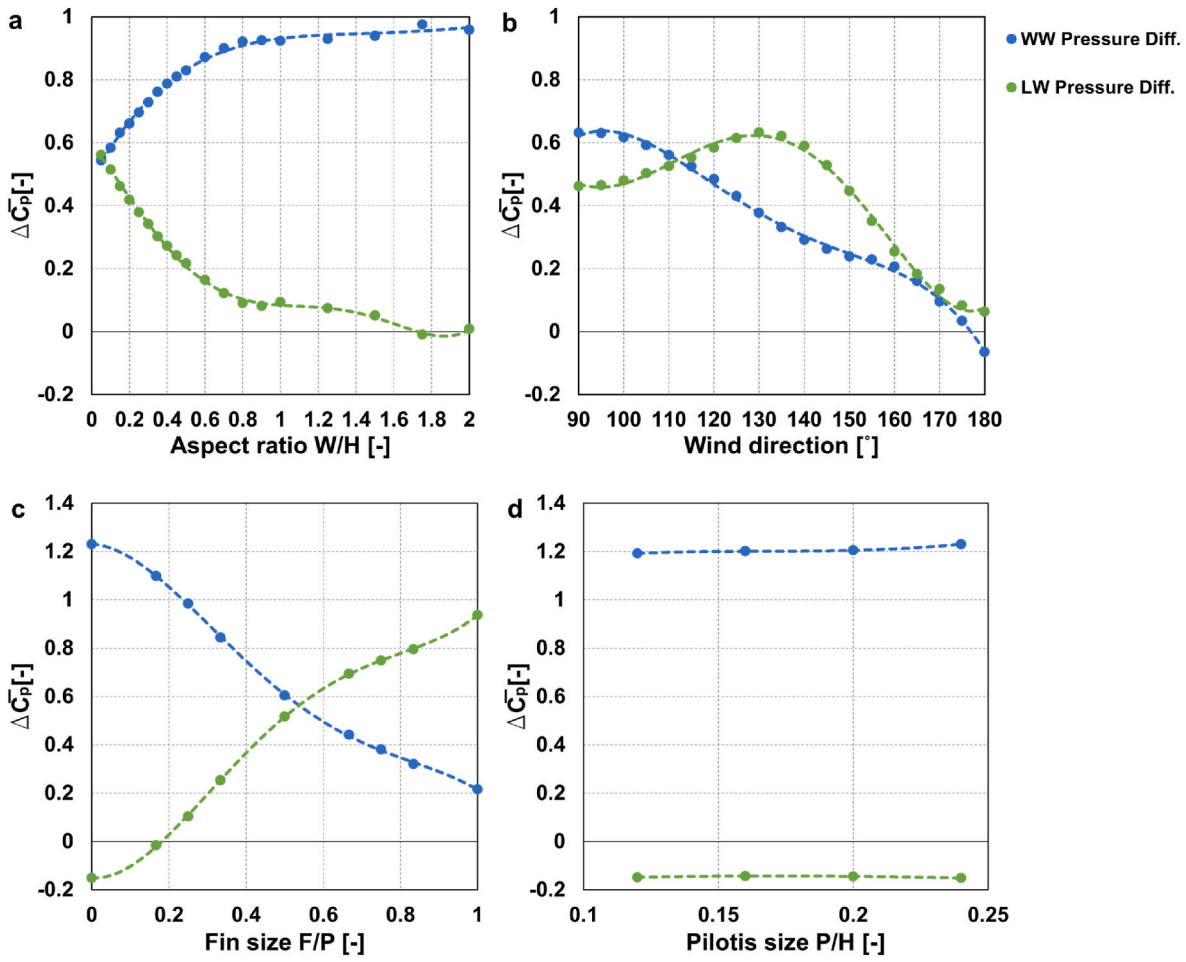

Fig. 12. Dimensionless differences of the averaged pressure coefficients on the windward and leeward sides of the building. (a) Aspect ratio (W/H) with a half-size wind fin; (b) Wind direction with an aspect ratio of 0.15; (c) Fin size with an aspect ratio of 0.15; (d) Pioitis size with an aspect ratio of 0.15.

increase in wind direction until almost none at 180°. The corresponding $\Delta\overline{C_{p_{LW}}}$ gradually increases at least until 130° and then it decreases until almost none at 180°. $\Delta\overline{C_{p_{WW}}}$ and $\Delta\overline{C_{p_{LW}}}$ are equalised around the wind direction of 110° with an aspect ratio of 0.15 W/H.

The size of the wind fin made a significant impact on C_p values on the internal walls of the void, and thus influences $\Delta\overline{C_p}$ on both sides (Fig. 12c). $\Delta\overline{C_{p_{WW}}}$ and $\Delta\overline{C_{p_{LW}}}$ are equalised around the fin size of 0.5 F/P. As shown in Fig. 12d, $\Delta\overline{C_p}$ on the two sides are a little sensitive to the size of pilotis. This is probably because the effect of pilotis size is primarily determined by the distance from the stagnation point located on the windward façade to the inlet of pilotis. As the distance increases, the volume of inflows to the pilotis would increase and thus influence $\Delta\overline{C_p}$ on the two sides of the building. Since the building height was uniform in the present study, the effects of the pilotios size was almost negligible.

The local sensitivity for the differences of the averaged pressure coefficients ($\Delta\overline{C_p}$) on the windward and leeward sides to the input design parameters is shown in Fig. 13. The local sensitivity of $\Delta\overline{C_p}$to the

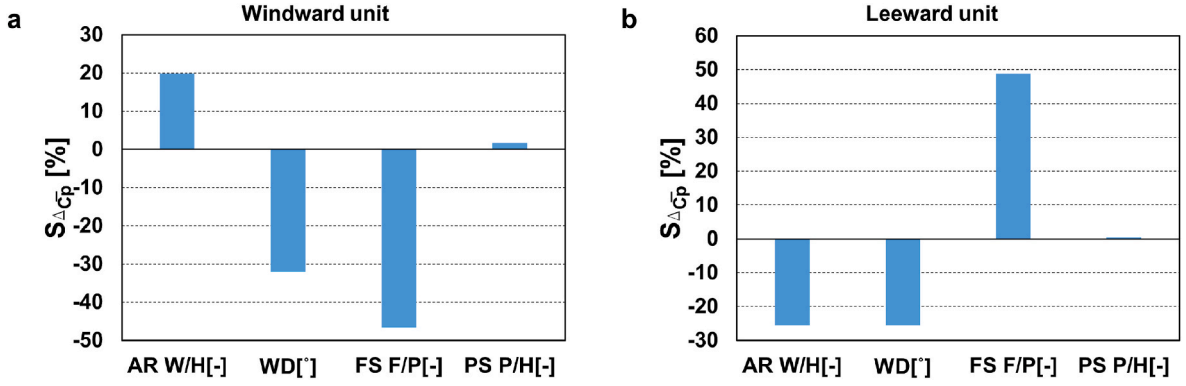

Fig. 13. Sensitivity of each parameter on the differences of the averaged pressure coefficients ($\Delta\overline{C_p}$) on the windward and leeward sides of the building. AR: Aspect ratio (W/H); WD: Wind direction; FS: Fin size (F/P); PS: Pilotis size (P/H).

input parameter X_i is defined as follows [74,75]:

$$S_{\Delta\overline{C_p}} = S_g \times \frac{max\left(\Delta\overline{C_{p_i}}\right) - min\left(\Delta\overline{C_{p_i}}\right)}{max\left(\Delta\overline{C_{p_{all}}}\right) - min\left(\Delta\overline{C_{p_{all}}}\right)} \times 100 S_g = \begin{cases} +1 \;\; if \;\; \dfrac{\partial\Delta\overline{C_{p_i}}}{\partial X_i} > 0 \\ -1 \;\; if \;\; \dfrac{\partial\Delta\overline{C_{p_i}}}{\partial X_i} < 0 \end{cases} \tag{13}$$

where $\Delta\overline{C_{pi}}$ is the difference of the averaged pressure coefficients calculated for the input parameter *i,* and $\Delta\overline{C_{p_{all}}}$ is that for all the input parameters. A positive sensitivity ($S_g > 0$) indicates that $\Delta\overline{C_p}$ is increased with the increase in the input parameter value, whereas a negative sensitivity ($S_g < 0$) indicates that $\Delta\overline{C_p}$ is decreased.

Fig. 13 presents the significant percentages of the impacts of the parameter change on $\Delta\overline{C_{p_{WW}}}$ and $\Delta\overline{C_{p_{LW}}}$ respectively. As shown, the parameters responsible for the variation of $\Delta\overline{C_{p_{WW}}}$ include fin size (−46%), wind direction (−31%) and aspect ratio (19%). Meanwhile, the corresponding parameters for $\Delta\overline{C_{p_{LW}}}$ are found to be fin size (48%), wind direction (−25%) and aspect ratio (−25%). The wind direction negatively influences $\Delta\overline{C_p}$ on both sides of the building as expected, but size of the wind fin and aspect ratio of the void influence the two sides of the building oppositely. This indicates that $\Delta\overline{C_p}$ on both sides of the building should be maximised by optimising the combinations of size of the wind fin and aspect ratio of the void under the specific prevailing wind directions.

6. Comparison of mass flow rate of building units

Fig. 14a illustrates the heat map of dimensionless MFR in the left side units (L), middle units (M) and right side units (R) on each floor level with various representative aspect ratios, wind directions and fin sizes, respectively (see Fig. 6). When the wind direction is 90° (perpendicular to the front façade), C_p was not flatly distributed especially on the windward external wall (Wall 1) (see Fig. 9b). This results in the non-uniform distribution of MFRs on the windward units (Fig. 14a,c). As the wind direction changes until its parallel to the front façade, the distribution of MFR changes on the windward side until 130° (Fig. 14b).

Fig. 15 shows the changes in average dimensionless MFR with the changes of aspect ratio *(W/H)*, wind direction and fin size *(F/P)*, respectively. As indicated in Fig. 15a, MFRs of both sides of the building are maximised simultaneously at the aspect ratio of 0.05–0.15 *W/H* with MFRs of 0.5–0.6. The MFRs on both sides of the building change until the aspect ratio of around 0.8 *W/H* in particular. Meanwhile, MFR on the windward side decreases from 0.6 to 0.25 with the increase in wind direction, whereas that of the leeward units increases from 0.5 to 0.6 until around 130° (Fig. 15b). After that, it decreases to 0.3 with the increase in wind direction until 180°. The MFRs between windward and leeward units are equalised at the wind direction of around 110°. The increase in fin size *(F/P)* decreases the average MFR from 0.8 to 0.4 for the windward units (Fig. 15c). In contrast, there is an increase in MFR from 0.3 to 0.7 for the leeward units after the fin size of around 0.2 *F/P*. The windward and leeward MFRs are identical at a fin size of 0.5 *F/P*.

7. Conclusion

This study intended to derive design critical for facilitating natural ventilation on the leeward side of the buildings. Validated CFD models of several interactions of the design elements were parametrically assessed to test the importance of sensitivity of the design parameters to expedite ventilation in both sides of double-loaded affordable housing. RANS Realizable k-ϵ turbulence model provides effective results for apartment buildings with vertical voids. The parametric study investigated the impacts of configurations of the proposed closed-vertical void on wind flow patterns inside the void and around the double-loaded apartment building, using the validated CFD models. The parameters included aspect ratio of the void *(W/H)*, wind direction, fin size *(F/P)* and pilotis size *(P/H)*. The local sensitivity analysis was also conducted to find how these parameters affected the ventilation performance of the building units. The following are the key conclusions that can be drawn:

- Unlike the ordinary open-vertical void, C_p inside the proposed closed-vertical void decreased with the increase in its aspect ratio

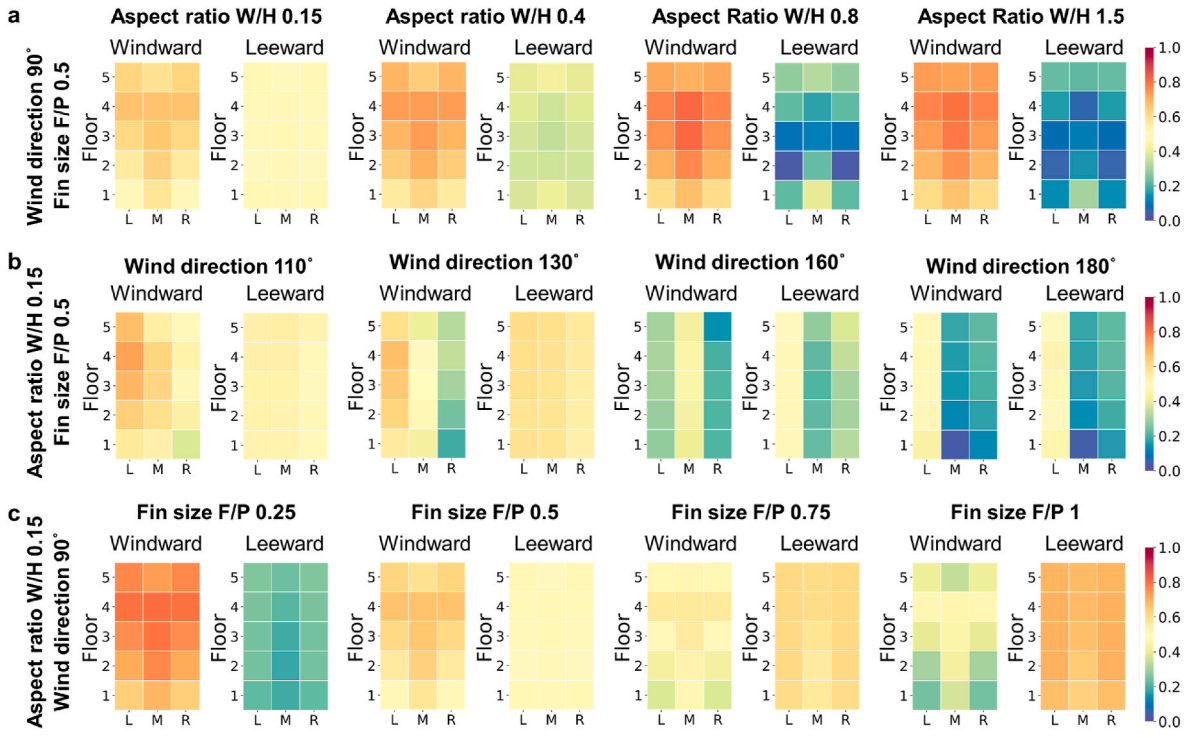

Fig. 14. Dimensionless mass flow rates on the windward and leeward units with various (a) aspect ratios, (b) wind direction and (c) fin size.

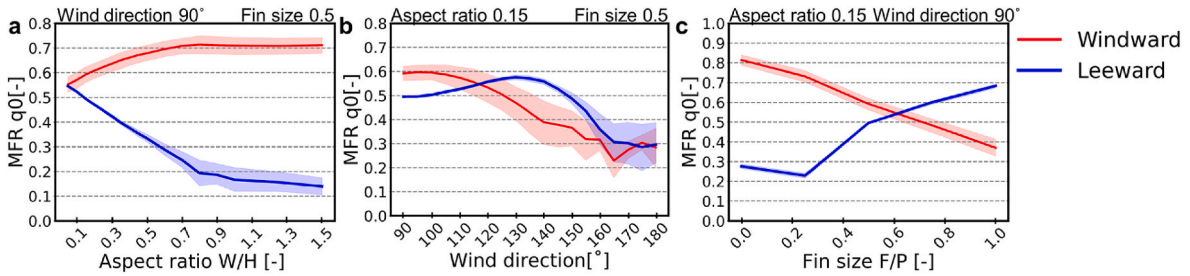

Fig. 15. Changes of dimensionless mass flow rates on the windward and leeward sides of the building with changes of (a) aspect ratios, (b) wind directions and (c) fin sizes. The standard aspect ratio is 0.15 that for wind direction is 90° and 0.5 for fin size. Error ranges indicate spatial distributions.

(W/H). This was primarily because while the volume of inflows was considered almost the same among cases with different aspect ratios, the volume of the void, which functioned as a reservoir, increased along with the aspect ratio. When the aspect ratio was small such as 0.15 *W/H*, the higher dynamic pressure was converted into the static pressure inside the void due to the flow resistance mainly caused by its closed rooftop. The dynamic pressure decreased with the increase in aspect ratio, and thus the converted static pressure inside the void, C_p, decreased accordingly. As the aspect ratio increased, the difference of C_p increased on the windward side of the building, while the corresponding C_p difference reduced on the leeward side especially until the aspect ratio of about 0.8 *W/H*. When the incident wind direction was 90°, the optimum aspect ratio was found to be 0.1–0.15 *W/H*.

- It was found that the increase in wind direction (i.e., from perpendicular to parallel to the front façade) reduced the differences of C_p on both sides of the building. However, the wind direction impacted the C_p distributions differently to the void walls on the windward and leeward sides. C_p values inside the void were almost constant from 90° to 130° and began declining until 180° because of the significant change in wind flow patterns in and around the building.
- The C_p values inside the void significantly increased with the increase in the size of the wind fin *(F/P)*. This was because the volume and wind speed of inflows in the void were effectively increased with the increased size of the fin. Nevertheless, the impacts of the fin size on C_p were different between the windward and leeward sides of the building. As the size of the wind fin increased, the difference of C_p decreased on the windward side, while the corresponding C_p difference increased on the leeward side. When the incident wind direction was 90°, the fin size of 0.5 *F/P* can be recommended to ensure adequate natural ventilation on both sides of the building. It was also found that the pilotis size *(P/H)* was not much influential to C_p on either side of the building.
- The sensitivity analysis results showed that the most influential parameter for the variation of C_p differences on the windward side of the building was the fin size with a contribution of −46%. The wind direction and aspect ratio of the void had −31% and 19%, respectively. The corresponding contributions for the leeward side were 48%, −25%, and −25% for fin size, wind direction, and aspect ratio, respectively. It was concluded that the differences of C_p and therefore MFR on both sides of the building could be maximised by optimising the combinations of the size of the wind fin and aspect ratio of the void under the specific prevailing wind directions.
- Mass flow rates in the assumed building units were calculated. As the aspect ratio *(W/H)* increased, MFRs increased on the windward side of the building while decreased on the leeward side. Two flow regimes were found in the regression lines with the aspect ratio. Until the aspect ratio of around 0.8 *W/H*, MFRs on both sides of the building changed almost linearly and after 0.8 *W/H*, the MFRs became stabilised. Overall, the increase in wind direction (from 90° to 180°) decreased MFRs on both sides of the building. However, the trend lines were not simple linear regressions, especially for the leeward side. On the leeward side, the MFRs slightly increased from 90° to around 130° and began declining especially until 160°. Meanwhile, as the size of the wind fin *(F/P)* increased, MFRs decreased linearly on the windward side while increasing on the leeward side from the fin size of 0.2 *F/P*.

These findings can be advanced using diverse building types with several interaction variables like thermal comfort and indoor air quality (IAQ) to evaluate the effectiveness of natural ventilation. This study is focused on the building design in the Global South (countries like India and Indonesia), which has predominantly tropical climatic conditions where the temperature is in a moderate range of 22 °C–35 °C. Basically, a complete passive cooling that we propose in this study can be applicable to the tropics except for the extreme hot conditions. However, detailed thermal comfort evaluation in specific climate conditions is necessary to ensure the applicability of the proposed ventilation technique. Meanwhile, the fresh air streams from the pilotis into the leeward units within the closed-vertical void design could potentially carry some exhaust air from the windward units to the leeward units across the void, posing an IAQ hazard. Under the current COVID-19 pandemic situation, it is urgently required to find the means to ensure sufficient ventilation rates to prevent infections while achieving indoor thermal comfort. However, carrying out such an investigation was beyond the scope of this work and could be included in future studies.

Overall, the results can help create sustainable design guidelines for improving natural ventilation by incorporating a closed-vertical void in affordable double-loaded apartment buildings. As affordability is still strongly required for social housing in developing countries, the passive cooling strategy should be prioritised. Nevertheless, if thermal comfort of the occupants cannot be achieved by the passive cooling techniques alone, then mechanical means such as efficient use of air-conditioning should be considered alternatively.

CRediT authorship contribution statement

Nikhil Kumar: Writing – original draft, Visualization, Validation, Software, Methodology, Investigation, Formal analysis. **Ronita Bardhan:** Methodology, Project administration, Supervision, Writing – review & editing. **Tetsu Kubota:** Writing – review & editing, Writing – original draft, Visualization, Validation, Supervision, Resources, Project administration, Methodology, Investigation, Funding acquisition, Formal analysis, Conceptualization. **Yoshihide Tominaga:** Formal analysis, Investigation, Methodology, Software, Supervision, Validation, Visualization, Writing – review & editing. **Mohammadreza Shirzadi:** Writing – review & editing, Visualization, Validation, Supervision, Software, Methodology, Formal analysis.

Declaration of competing interest

The authors declare that they have no known competing financial interests or personal relationships that could have appeared to influence the work reported in this paper.

Acknowledgments

This research was partially supported by the Science and Technology Research Partnership for Sustainable Development (SATREPS) in collaboration with Japan Science and Technology Agency (JST, JPMJSA1904) and Japan International Cooperation Agency (JICA). We also highly acknowledge the supports from the YKK AP Inc. and the Asahi Glass Foundation. Nikhil Kumar would like to acknowledge the Ministry of Human Resource and Development (MHRD), India and the International Linkage Degree Program (ILDP) scholarship by Hiroshima University, Japan for providing all necessary support.

References

[1] G. Baruch, Climate Considerations in Building and Urban Design, John Wiley & Sons, Ltd, Chichester, UK, 1998. https://www.wiley.com/en-us/Climate+Considerations+in+Building+and+Urban+Design-p-9780471291770.
[2] N. Kumar, T. Kubota, R. Bardhan, Y. Tominaga, CFD analysis of airflow in voids for better cross ventilation in midrise buildings in hot and humid climates, Proc. 16th Int. Build. Perform. Simul. Assoc. (2019) 3879–3885.
[3] R. Debnath, R. Bardhan, M. Sunikka-Blank, How does slum rehabilitation influence appliance ownership? A structural model of non-income drivers, Energy Pol. 132 (2019) 418–428, https://doi.org/10.1016/j.enpol.2019.06.005.
[4] R. Debnath, G.M.F. Simoes, R. Bardhan, S.M. Leder, R. Lamberts, M. Sunikka-Blank, Energy justice in slum rehabilitation housing: an empirical exploration of built environment effects on socio-cultural energy demand, Sustainability 12 (2020) 3027, https://doi.org/10.3390/su12073027.
[5] R. Bardhan, R. Debnath, J. Malik, A. Sarkar, Low-income housing layouts under socio-architectural complexities: a parametric study for sustainable slum rehabilitation, Sustain. Cities Soc. 41 (2018) 126–138, https://doi.org/10.1016/j.scs.2018.04.038.
[6] P. Pardeshi, B. Jadhav, R. Singh, N. Kapoor, R. Bardhan, A. Jana, S. David, N. Roy, Association between Architectural Parameters and Burden of Tuberculosis in Three Resettlement Colonies of M-East Ward, Cities Heal, Mumbai, India, 2020, pp. 1–18, https://doi.org/10.1080/23748834.2020.1731919, 00.
[7] J. Lueker, R. Bardhan, A. Sarkar, L. Norford, Indoor air quality among Mumbai's resettled populations: comparing Dharavi slum to nearby rehabilitation sites, Build. Environ. 167 (2020) 106419, https://doi.org/10.1016/j.buildenv.2019.106419.
[8] N.K. Bansal, R. Mathur, M.S. Bhandari, A study of solar chimney assisted wind tower system for natural ventilation in buildings, Build. Environ. 29 (1994) 495–500, https://doi.org/10.1016/0360-1323(94)90008-6.
[9] Y. Li, A. Delsante, J. Symons, Prediction of natural ventilation in buildings with large openings, Build. Environ. 35 (2000) 191–206, https://doi.org/10.1016/S0360-1323(99)00011-6.
[10] Y. Jiang, D. Alexander, H. Jenkins, R. Arthur, Q. Chen, Natural ventilation in buildings: measurement in a wind tunnel and numerical simulation with large-eddy simulation, J. Wind Eng. Ind. Aerod. 91 (2003) 331–353, https://doi.org/10.1016/S0167-6105(02)00380-X.
[11] Y. Jiang, Q. Chen, Study of natural ventilation in buildings by large eddy simulation, J. Wind Eng. Ind. Aerod. 89 (2001) 1155–1178, https://doi.org/10.1016/S0167-6105(01)00106-4.
[12] G. Evola, V. Popov, Computational analysis of wind driven natural ventilation in buildings, Energy Build. 38 (2006) 491–501, https://doi.org/10.1016/j.enbuild.2005.08.008.
[13] C. Zhou, Z. Wang, Q. Chen, Y. Jiang, J. Pei, Design optimization and field demonstration of natural ventilation for high-rise residential buildings, Energy Build. 82 (2014) 457–465, https://doi.org/10.1016/j.enbuild.2014.06.036.
[14] A. Aflaki, N. Mahyuddin, Z. Al-Cheikh Mahmoud, M.R. Baharum, A review on natural ventilation applications through building façade components and ventilation openings in tropical climates, Energy Build. 101 (2015) 153–162, https://doi.org/10.1016/j.enbuild.2015.04.033.
[15] G.A. Faggianelli, A. Brun, E. Wurtz, M. Muselli, Natural cross ventilation in buildings on Mediterranean coastal zones, Energy Build. 77 (2014) 206–218, https://doi.org/10.1016/j.enbuild.2014.03.042.
[16] S. Omrani, V. Garcia-Hansen, B. Capra, R. Drogemuller, Natural ventilation in multi-storey buildings: design process and review of evaluation tools, Build. Environ. 116 (2017) 182–194, https://doi.org/10.1016/j.buildenv.2017.02.012.
[17] N. Kumar, T. Kubota, Y. Tominaga, M. Shirzadi, R. Bardhan, CFD simulations of wind-induced ventilation in apartment buildings with vertical voids: effects of pilotis and wind fin on ventilation performance, Build. Environ. 194 (2021) 107666, https://doi.org/10.1016/j.buildenv.2021.107666.
[18] L. Wai, L.K. Norford, Pedestrian-level wind speed enhancement with void decks in three-dimensional urban street canyons, Build, Environ. Times 155 (2019) 399–407, https://doi.org/10.1016/j.buildenv.2019.03.058.
[19] L. Wai, L.K. Norford, Pedestrian-level wind speed enhancement in urban street canyons with void decks, Build. Environ. 146 (2018) 64–76, https://doi.org/10.1016/j.buildenv.2018.09.039.
[20] T.G. Farea, D.R. Ossen, S. Alkaff, H. Kotani, CFD modeling for natural ventilation in a lightwell connected to outdoor through horizontal voids, Energy Build. 86 (2015) 502–513, https://doi.org/10.1016/j.enbuild.2014.10.030.
[21] F. Muhsin, W.F.M. Yusoff, M.F. Mohamed, A.R. Sapian, CFD modeling of natural ventilation in a void connected to the living units of multi-storey housing for thermal comfort, Energy Build. 144 (2017) 1–16, https://doi.org/10.1016/j.enbuild.2017.03.035.
[22] F. Muhsin, W. Mohammad Yusoff, M. Mohamed, A. Sapian, The effects of void on natural ventilation performance in multi-storey housing, Buildings 6 (2016) 35, https://doi.org/10.3390/buildings6030035.
[23] F. Muhsin, W.F.M. Yusoff, M.F. Mohamed, A.R. Sapian, CFD modeling of natural ventilation in a void connected to the living units of multi-storey housing for thermal comfort, Energy Build. 144 (2017) 1–16, https://doi.org/10.1016/j.enbuild.2017.03.035.
[24] F. Muhsin, W. Fatimah, M. Yusoff, M.F. Mohamed, M. Rasidi, M. Rasani, A. R. Sapian, Potential of voids to enhance natural ventilation in medium cost multi-storey housing (MCMSH) for hot and humid climate, ARPN J. Eng. Appl. Sci. 12 (2017) 3137–3144. http://www.arpnjournals.org/jeas/research_papers/rp_2017/jeas_0517_6022.pdf.
[25] J. Hang, Z. Luo, M. Sandberg, J. Gong, Natural ventilation assessment in typical open and semi-open urban environments under various wind directions, Build. Environ. 70 (2013) 318–333, https://doi.org/10.1016/j.buildenv.2013.09.002.
[26] X. Zhang, A.U. Weerasuriya, K.T. Tse, CFD simulation of natural ventilation of a generic building in various incident wind directions: comparison of turbulence modelling, evaluation methods, and ventilation mechanisms, Energy Build. 229 (2020) 110516, https://doi.org/10.1016/j.enbuild.2020.110516.
[27] K. Ahmad, M. Khare, K.K. Chaudhry, Wind tunnel simulation studies on dispersion at urban street canyons and intersections - a review, J. Wind Eng. Ind. Aerod. 93 (2005) 697–717, https://doi.org/10.1016/j.jweia.2005.04.002.
[28] T.R. Oke, G. Mills, A. Christen, J.A. Voogt, Urban Climates, Cambridge University Press, 2017, https://doi.org/10.1017/9781139016476.
[29] A. Saltelli, M. Ratto, T. Andres, F. Campolongo, J. Cariboni, D. Gatelli, M. Saisana, S. Tarantola, Global Sensitivity Analysis, WILEY, 2008, https://doi.org/10.1111/j.1751-5823.2008.00062_17.x.
[30] C. Ghiaus, F. Allard, M. Santamouris, C. Georgakis, F. Nicol, Urban environment influence on natural ventilation potential, Build. Environ. 41 (2006) 395–406, https://doi.org/10.1016/j.buildenv.2005.02.003.
[31] B. Xie, Y. Han, H. Huang, L. Chen, Y. Zhou, C. Fan, X. Liu, Numerical study of natural ventilation in urban shallow tunnels: impact of shaft cross section, Sustain. Cities Soc. 42 (2018) 521–537, https://doi.org/10.1016/j.scs.2018.07.022.
[32] F. Allard, C. Ghiaus, Natural Ventilation in the Urban Environment, 2005. Earthscan.
[33] J. Hang, Z. Xian, D. Wang, C.M. Mak, B. Wang, Y. Fan, The impacts of viaduct settings and street aspect ratios on personal intake fraction in three-dimensional urban-like geometries, Build, Environ. Times 143 (2018) 138–162, https://doi.org/10.1016/j.buildenv.2018.07.001.
[34] H. Qin, P. Lin, S.S.Y. Lau, D. Song, Influence of site and tower types on urban natural ventilation performance in high-rise high-density urban environment, Build. Environ. 179 (2020) 106960, https://doi.org/10.1016/j.buildenv.2020.106960.
[35] S.H.L. Yim, J.C.H. Fung, A.K.H. Lau, S.C. Kot, Air ventilation impacts of the "wall effect" resulting from the alignment of high-rise buildings, Atmos. Environ. 43 (2009) 4982–4994, https://doi.org/10.1016/j.atmosenv.2009.07.002.
[36] L. Chen, J. Hang, M. Sandberg, L. Claesson, S. Di Sabatino, H. Wigo, The impacts of building height variations and building packing densities on flow adjustment and city breathability in idealized urban models, Build. Environ. 118 (2017) 344–361, https://doi.org/10.1016/j.buildenv.2017.03.042.
[37] C. Ding, K.P. Lam, Data-driven model for cross ventilation potential in high-density cities based on coupled CFD simulation and machine learning, Build. Environ. 165 (2019) 106394, https://doi.org/10.1016/j.buildenv.2019.106394.
[38] A.Z. Dhunny, N. Samkhaniani, M.R. Lollchund, S.D.D.V. Rughooputh, Investigation of multi-level wind flow characteristics and pedestrian comfort in a tropical city, Urban Clim. 24 (2018) 185–204, https://doi.org/10.1016/j.uclim.2018.03.002.
[39] C.W. Tsang, K.C.S. Kwok, P.A. Hitchcock, Wind tunnel study of pedestrian level wind environment around tall buildings: effects of building dimensions, separation and podium, Build. Environ. 49 (2012) 167–181, https://doi.org/10.1016/j.buildenv.2011.08.014.
[40] Y. He, A. Tablada, N.H. Wong, Effects of non-uniform and orthogonal breezeway networks on pedestrian ventilation in Singapore's high-density urban environments, Urban Clim. 24 (2018) 460–484, https://doi.org/10.1016/j.uclim.2017.03.005.
[41] M. Alsailani, H. Montazeri, A. Rezaeiha, Towards optimal aerodynamic design of wind catchers: impact of geometrical characteristics, Renew. Energy 168 (2021) 1344–1363, https://doi.org/10.1016/j.renene.2020.12.053.
[42] S. Omrani, V. Garcia-Hansen, B.R. Capra, R. Drogemuller, On the effect of provision of balconies on natural ventilation and thermal comfort in high-rise residential buildings, Build. Environ. 123 (2017) 504–516, https://doi.org/10.1016/j.buildenv.2017.07.016.
[43] F. Jomehzadeh, H.M. Hussen, J.K. Calautit, P. Nejat, M.S. Ferwati, Natural ventilation by windcatcher (Badgir): a review on the impacts of geometry, microclimate and macroclimate, Energy Build. 226 (2020) 110396, https://doi.org/10.1016/j.enbuild.2020.110396.
[44] X. Zheng, H. Montazeri, B. Blocken, CFD analysis of the impact of geometrical characteristics of building balconies on near-façade wind flow and surface pressure, Build. Environ. 200 (2021) 107904, https://doi.org/10.1016/j.buildenv.2021.107904.
[45] G.V. Fracastoro, G. Mutani, M. Perino, Experimental and theoretical analysis of natural ventilation by windows opening, Energy Build. 34 (2002) 817–827, https://doi.org/10.1016/S0378-7788(02)00099-3.
[46] M. Santamouris, A. Synnefa, M. Asssimakopoulos, I. Livada, K. Pavlou, M. Papaglastra, N. Gaitani, D. Kolokotsa, V. Assimakopoulos, Experimental

investigation of the air flow and indoor carbon dioxide concentration in classrooms with intermittent natural ventilation, Energy Build. 40 (2008) 1833–1843, https://doi.org/10.1016/j.enbuild.2008.04.002.
[47] C.F. Gao, W.L. Lee, Evaluating the influence of openings configuration on natural ventilation performance of residential units in Hong Kong, Build. Environ. 46 (2011) 961–969, https://doi.org/10.1016/j.buildenv.2010.10.029.
[48] Y.W. Fung, W.L. Lee, Identifying the most influential parameter affecting natural ventilation performance in high-rise high-density residential buildings, Indoor Built Environ. 24 (2015) 803–812, https://doi.org/10.1177/1420326X14536189.
[49] P. Heiselberg, H. Brohus, A. Hesselholt, H. Rasmussen, E. Seinre, S. Thomas, Application of sensitivity analysis in design of sustainable buildings, Renew. Energy 34 (2009) 2030–2036, https://doi.org/10.1016/j.renene.2009.02.016.
[50] Z. Pang, Z. O'Neill, Y. Li, F. Niu, The role of sensitivity analysis in the building performance analysis: a critical review, Energy Build. 209 (2020) 109659, https://doi.org/10.1016/j.enbuild.2019.109659.
[51] B. Iooss, P. Lemaître, Uncertainty management in simulation-optimization of complex systems, Oper. Res. Comput. Sci. Interfaces Ser. 59 (2015) 101–122, https://doi.org/10.1007/978-1-4899-7547-8.
[52] A. Saltelli, P. Annoni, How to avoid a perfunctory sensitivity analysis, Environ. Model. Software 25 (2010) 1508–1517, https://doi.org/10.1016/j.envsoft.2010.04.012.
[53] A.P. de A. Rocha, J. Goffart, L. Houben, N. Mendes, On the uncertainty assessment of incident direct solar radiation on building facades due to shading devices, Energy Build. 133 (2016) 295–304, https://doi.org/10.1016/j.enbuild.2016.09.058.
[54] K. Menberg, Y. Heo, R. Choudhary, Sensitivity analysis methods for building energy models: comparing computational costs and extractable information, Energy Build. 133 (2016) 433–445, https://doi.org/10.1016/j.enbuild.2016.10.005.
[55] Y. Tominaga, A. Mochida, R. Yoshie, H. Kataoka, T. Nozu, M. Yoshikawa, T. Shirasawa, AIJ guidelines for practical applications of CFD to pedestrian wind environment around buildings, J. Wind Eng. Ind. Aerod. 96 (2008) 1749–1761, https://doi.org/10.1016/j.jweia.2008.02.058.
[56] B.E. Launder, D.B. Spalding, The Numerical Computation of Turbulent Flows, Pergamon Press, Ltd, 1983, https://doi.org/10.1016/b978-0-08-030937-8.50016-7.
[57] B. Blocken, J. Carmeliet, T. Stathopoulos, CFD evaluation of wind speed conditions in passages between parallel buildings-effect of wall-function roughness modifications for the atmospheric boundary layer flow, J. Wind Eng. Ind. Aerod. 95 (2007) 941–962, https://doi.org/10.1016/j.jweia.2007.01.013.
[58] B. Blocken, T. Stathopoulos, J. Carmeliet, CFD simulation of the atmospheric boundary layer: wall function problems, Atmos. Environ. 41 (2007) 238–252, https://doi.org/10.1016/j.atmosenv.2006.08.019.
[59] K.J. Fidkowski, D.L. Darmofal, A triangular cut-cell adaptive method for high-order discretizations of the compressible Navier-Stokes equations, J. Comput. Phys. 225 (2007) 1653–1672, https://doi.org/10.1016/j.jcp.2007.02.007.
[60] T.-H. Shih, W.W. Liou, A. Shabbir, Z. Yang, J. Zhu, A new kappa-epsilon eddy viscosity model for high Reynolds number turbulent flows, Comput. Fluids 24 (1995) 227–238, https://doi.org/10.1007/978-3-319-27386-0_7.
[61] B.M. Jones, M.J. Cook, S.D. Fitzgerald, C.R. Iddon, A review of ventilation opening area terminology, Energy Build. 118 (2016) 249–258, https://doi.org/10.1016/j.enbuild.2016.02.053.
[62] M. Shirzadi, P.A. Mirzaei, M. Naghashzadegan, Development of an adaptive discharge coefficient to improve the accuracy of cross-ventilation airflow calculation in building energy simulation tools, Build. Environ. 127 (2018) 277–290, https://doi.org/10.1016/j.buildenv.2017.10.019.
[63] P.J. Roache, Quantification of uncertainty in computational fluid dynamics, Annu. Rev. Fluid Mech. 29 (1997) 123–160, https://doi.org/10.1146/annurev.fluid.29.1.123.
[64] S. Akabayashi, A. Mochida, Y. Tominaga, M. Yoshida, J. Sakaguchi, Performance of new wind tunnel of Niigata Institute of Technology, J. Wind Eng. 68 (1996) 95–106.
[65] R. Yoshie, A. Mochida, Y. Tominaga, H. Kataoka, K. Harimoto, T. Nozu, T. Shirasawa, Cooperative project for CFD prediction of pedestrian wind environment in the Architectural Institute of Japan, J. Wind Eng. Ind. Aerod. 95 (2007) 1551–1578, https://doi.org/10.1016/j.jweia.2007.02.023.
[66] T. Kubota, M. Miura, Y. Tominaga, A. Mochida, Wind tunnel tests on the relationship between building density and pedestrian-level wind velocity: Development of guidelines for realizing acceptable wind environment in residential neighborhoods, Build, Environ. Times 43 (2008) 1699–1708, https://doi.org/10.1016/j.buildenv.2007.10.015.
[67] M. Shirzadi, Y. Tominaga, P.A. Mirzaei, Experimental study on cross-ventilation of a generic building in highly-dense urban areas: impact of planar area density and wind direction, J. Wind Eng. Ind. Aerod. 196 (2020) 104030, https://doi.org/10.1016/j.jweia.2019.104030.
[68] M. Shirzadi, Y. Tominaga, P.A. Mirzaei, Wind tunnel experiments on cross-ventilation flow of a generic sheltered building in urban areas, Build. Environ. 158 (2019) 60–72, https://doi.org/10.1016/j.buildenv.2019.04.057.
[69] Y. Tominaga, S. ichi Akabayashi, T. Kitahara, Y. Arinami, Air flow around isolated gable-roof buildings with different roof pitches: wind tunnel experiments and CFD simulations, Build. Environ. 84 (2015) 204–213, https://doi.org/10.1016/j.buildenv.2014.11.012.
[70] M.T. Puth, M. Neuhäuser, G.D. Ruxton, Effective use of Pearson's product-moment correlation coefficient, Anim. Behav. 93 (2014) 183–189, https://doi.org/10.1016/j.anbehav.2014.05.003.
[71] D. Golubić, W. Meile, G. Brenn, H. Kozmar, Wind-tunnel analysis of natural ventilation in a generic building in sheltered and unsheltered conditions: impact of Reynolds number and wind direction, J. Wind Eng. Ind. Aerod. 207 (2020), https://doi.org/10.1016/j.jweia.2020.104388.
[72] M.V. Cruz-Salas, J.A. Castillo, G. Huelsz, Effect of windexchanger duct cross-section area and geometry on the room airflow distribution, J. Wind Eng. Ind. Aerod. 179 (2018) 514–523, https://doi.org/10.1016/j.jweia.2018.06.022.
[73] H. Montazeri, F. Montazeri, R. Azizian, S. Mostafavi, Two-sided wind catcher performance evaluation using experimental, numerical and analytical modeling, Renew. Energy 35 (2010) 1424–1435, https://doi.org/10.1016/j.renene.2009.12.003.
[74] M. Shirzadi, Y. Tominaga, Multi-fidelity shape optimization methodology for pedestrian-level wind environment, Build. Environ. (2021) 108076, https://doi.org/10.1016/j.buildenv.2021.108076.
[75] M. Aelaei, S. Karimian, F. Ommi, Sensitivity analysis and optimization of delta wing design parameters using CFD-based response surface method, J. Appl. Fluid Mech. 12 (2019) 1885–1903, https://doi.org/10.29252/JAFM.12.06.29706.